

## Feature Article

# Ultra-low refractive index mesoporous substrates for waveguide structures

D. Konjhodzic<sup>1</sup>, S. Schröter<sup>2</sup>, and F. Marlow<sup>\*,1</sup>

<sup>1</sup> Max-Planck-Institut für Kohlenforschung, Kaiser-Wilhelm-Platz 1, 45470 Mülheim an der Ruhr, Germany

<sup>2</sup> Institut für Physikalische Hochtechnologie Jena e.V., A. Einstein Str. 9, 07745 Jena, Germany

Received 15 March 2007, revised 23 May 2007, accepted 15 June 2007

Published online 30 October 2007

PACS 42.79.Gn, 68.37.–d, 68.55.–a, 78.20.Ci, 81.20.Fw

Mesoporous silica films were synthesized by dip-coating. In this process, evaporation induced self-assembly leads to the formation of an ordered pore structure. Two types of films with different optical properties have been found in dependence on the humidity during the synthesis. The synthesis field has been explored in order to locate optically perfect films. Both film types, denoted as A and B, have been characterized by small angle X-ray scattering (SAXS), transmission electron microscopy (TEM) and atomic force microscopy (AFM). From these results, the different structures for the two film types have been determined. A-type films have a stable worm-like structure, whereas for B-type films a sustained lamellar structure has been found. A very low refractive index has been measured for A-type films and its stability has been examined. These films have been used as low- $n$  supports to realize waveguide structures based on polymers, Ta<sub>2</sub>O<sub>5</sub>, and the ferroelectric material PZT.

© 2007 WILEY-VCH Verlag GmbH & Co. KGaA, Weinheim

## 1 Introduction

Mesoporous materials have pore sizes between 2 and 50 nm and have been studied for potential applications in catalysis, separation, and chemical sensing in many works since their discovery in 1992. The use of these materials as novel optical or electrical materials has also attracted a high interest. They could be a component in one of the next generations of chips [1]. Here, low dielectric constants are required and mesoporous materials can exploit their high porosity for achieving this. It is expected that these materials can substantially help to overcome the problems of cross-talk and propagation delay. The semiconductor industry is currently targeting new dielectric films with dielectric constants  $k = 2.5$  to 3.0, and it is anticipated that, as the packing density of metal lines on the semiconductors continues to increase, interlevel dielectric films with ultra-low  $k$  ( $k < 2.2$ ) will soon be required [1].

In the field of integrated optics, a similar materials problem is emerging. Waveguides with many functions are designed, but they all need a support with a lower refractive index to operate properly. Many of new interesting waveguides (e.g. 2D PhCs) have unfortunately relatively low effective refractive indices, demanding even lower support indices. Low- $n$  materials have nearly the same requirements as low- $k$  materials. They differ in the relevant frequency range leading to the decisive role of OH groups and water for the low- $k$  materials. Both applications require perfect films of these materials.

\* Corresponding author: e-mail: marlow@mpi-muelheim.mpg.de, Phone: +49 208 306 2407, Fax: +49 208 306 2995

In this work we describe an optimized fabrication procedure of mesoporous silica films and analyze the properties of these mesoporous films. The films are used as ultra low- $n$  support for the realization of the polymeric or inorganic waveguides.

The use of such low- $n$  supports could be decisive step towards optical integrated circuits on a highly variable material basis because the index contrast between the guiding and the support layer is then easy to achieve. The refractive-index contrast is very important for dielectric multilayer structures, optical resonators, and photonic crystals. In integrated optics, low- $n$  materials would be very helpful to enable more waveguiding structures.

There have been a number of recent studies on the application of porous xerogel [2] or mesoporous silica films [3] as low- $k$  materials. Optically applicable xerogel films for waveguide cladding layers were prepared using an ethylene glycol co-solvent procedure and the core layer was prepared using plasma-enhanced chemical vapor-deposited silicon dioxide or a siloxane epoxy polymer. These polymer-xerogel waveguides had a maximum refractive index contrast of 0.34, whereas the PECVD oxide-xerogel planar waveguides were fabricated with a maximum refractive index contrast of only 0.28. A low dielectric constant of 1.8 to 2.5 was measured for the spin-coated mesoporous silica films [3], but no realization of the waveguides with this system was reported so far.

## 2 Mesoporous films

### 2.1 Fabrication of mesoporous silica films

#### 2.1.1 General remarks

Ordered mesoporous materials are made with the use of surfactants forming micelles and acting as structure-directing agent (SDA). This kind of templating approach was used in the MCM-41 synthesis for the first time [4]. The ordered mesophase depends on the concentrations of surfactant, the inorganic species, and the processing conditions. The mechanism for the molecular interaction between an inorganic material and a surfactant was first discussed by Beck et al. [5] in detail. They proposed two alternative pathways, in which either the liquid-crystal phase is intact before the silica species are added, or the addition of the silica results in the ordering of the silica-encased surfactant micelles. In this case, silica species coat the surface of surfactant micelles, which then self-order to form the phase observed in the final product. The final porous structure is obtained after removal of the organic template upon thermal treatment called calcination.

Thin films of such mesoporous materials can be realized in a dip-coating process [6]. The solution deposited on the supports contains metal-alkoxide as a precursor and surfactant as a SDA. The film thickness is controlled by the evaporation rate of the solvent, the drawing speed, and by the viscosity of the coating solution. The increase in surfactant concentration upon solvent evaporation causes the assembly process of the micelles into a close-packed phase.

A special class of mesoporous materials named SBA-15 has been synthesized by use of amphiphilic triblock-copolymers [7]. The SBA-15 materials are formed in acidic media and show mostly two-dimensional hexagonal (space group  $p6mm$ ) mesophases consisting of a silica channel framework filled with the block-copolymer. Calcination gives porous silica structures with relatively large lattice constants of 7.5 nm. These materials are highly versatile and can also be used in low- $k$  and low- $n$  applications.

#### 2.1.2 Preparation details

A solution containing the triblock copolymer poly(ethylene oxide)-block-poly(propylene oxide)-block-poly(ethylene oxide) (P123,  $\text{EO}_{20}\text{PO}_{70}\text{EO}_{20}$ ), ethanol, water, HCl, and Rhodamine 6G was mixed with tetrabutyl orthosilicate (TBOS) as a silica precursor resulting in the final molar composition: TBOS: P123:  $\text{H}_2\text{O}$ : HCl: EtOH: Rh6G = 1:0.018:2.83:0.015:5.58:0.0009. A pre-reaction of this solution has been carried out for 2.5 h at 70 °C. The solution was deposited onto carefully cleaned substrates (BK7 glass slides, Si-wafer, mica slides, or epoxy resin blocks) by dip-coating. The porosity of the films was obtained by calcination. The thickness of the resulting transparent films was tuned in the range 300–1100 nm.

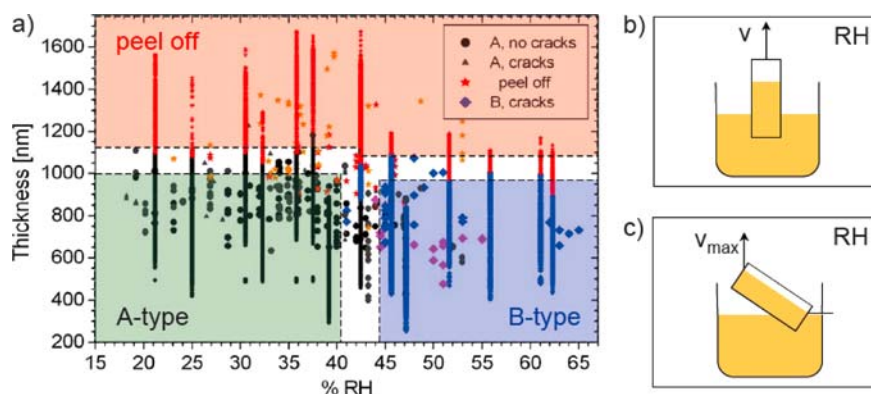


**Fig. 1** (online colour at: [www.pss-a.com](http://www.pss-a.com)) a) Synthesis field. The green region shows mainly the A-type films and the blue region the B-type films. In the red region the films start to peel off. Schemes for b) normal dip coating and c) coating with tilted movement.

According to their visual appearance, two types of films have been observed and denoted as A-type and B-type [8]. A-type films are perfectly clear, whereas B-type films appear slightly milky. Observation with an optical microscope revealed homogeneously distributed, bubble-like defects between  $1 \mu\text{m}$  and  $100 \mu\text{m}$  in size for B-type films, whereas the A-type films are fully non-structured. These two types of films were found in dependence on the processing conditions. A-type films turned out to be well suited as low- $n$  supports and were used in Ref. [9], whereas B-type films revealed some academically interesting features.

The most important processing parameter which determines the film type is humidity of the surrounding air. In order to obtain perfect A-type films it is crucial to keep the relative humidity (RH) on a low level during the synthesis. For this, an air conditioner system was used. During the film deposition the relative humidity in the chamber fluctuated about  $\pm 4\%$ , due to opening of the chamber for the sample exchange.

The realized film thickness and the relative humidity during the film deposition form a synthesis field depicted in Fig. 1. Single points in the diagram represent the samples synthesized with the normal dip-coating. The lines in the diagram represent samples with thickness gradient deposited by a tilting movement with the substrate. This process results in the whole range of the thicknesses at a certain value of the relative humidity.

One can distinguish three regions in the diagram. Clear A-type films (black circles) appear predominantly in the region of relative humidities below about 41% RH and thicknesses below about 1000 nm. B-type films appear predominantly in the region above about 44% RH and with thicknesses below about 970 nm. Films with ablations for both film types (red stars) are to be found mainly in the region above 1100 nm (red region). In white regions no one of these regions could be precisely assigned. The region between A-type and B-type of 4% RH width, where both film types occur, can be explained with the typical fluctuations of the relative humidity ( $\pm 4\%$ ) during the film synthesis.

## 2.2 Characterization and structure determination of MSFs

To determine the structures, small angle X-ray scattering (SAXS), transmission electron microscopy (TEM), and atomic force microscopy (AFM) investigations were performed.

As-synthesized A-type films showed a circle-like X-ray diffraction pattern with a radius of  $2\theta = 1.08^\circ$  (8.2 nm) and an isotropic intensity distribution (Fig. 2a). In brackets we give the deduced lattice constant as a result of application of the Bragg equation. After calcination an ellipse with the half axes of  $1.08^\circ$  (8.2 nm) and  $1.95^\circ$  (4.5 nm) was found (Fig. 2b). This diffraction pattern can be attributed to a partial ordering of uniform channels with well-defined pore sizes. The structure shrinks in the direction normal to the surface upon calcination. This effect is visible in the longer half-axis in the diffraction pattern and amounts to 55% [8].

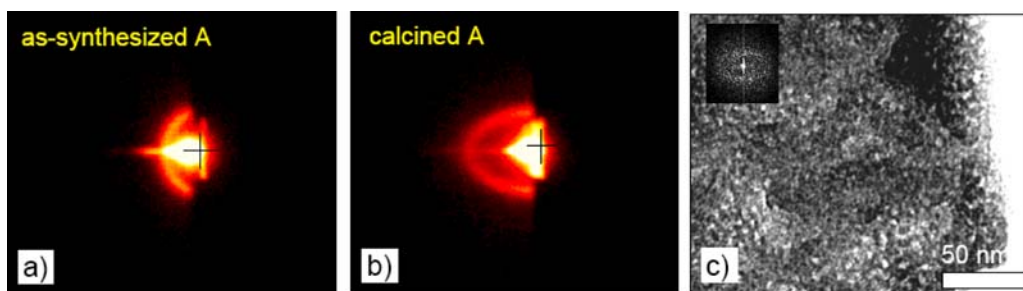


**Fig. 2** (online colour at: [www.pss-a.com](http://www.pss-a.com)) Structure determination of A-type films. a) The SAXS diffraction pattern of as-synthesized and b) calcined films. The right sides of diffraction patterns are not accessible by the scattered waves. The sample was positioned perpendicular to the image plane in vertical direction. The primary beam position is marked by a cross. c) TEM micrograph of the cross-section of a calcined A-type film. Scale bar: 50 nm, Inset: FFT [8].

The TEM analysis was performed on cross sections of the samples. The resulting micrograph (Fig. 2c) shows fluctuating pattern typical for the so-called worm-like structure [10]. It can be imagined as nearly dense-packed bundles of long flexible rods (Fig. 5a). This structure can be considered as a non-equilibrium state of a dense-packed channel array. The equilibrium state would be the hexagonal phase. One may speculate if this partially disordered structure is useful for the application as low- $n$  film. Many authors have reported similar films but there are no reliable facts that the synthesized films are really thick enough, i.e. thicker than 1  $\mu\text{m}$ , and defect-free. For a number of syntheses it must be recognized that there are unsolved difficulties if the films becomes thicker than 400 nm. This is, however, too thin for an optical application because the evanescent fields penetrate deeper into the film. Much synthesis work was focused on perfect and, therefore, especially nice structures. However, these nice and highly ordered structures are not so well suited for surviving the stress during the film synthesis because the structure has no freedom to change without destruction. A partially disordered structure allows a more flexible reaction to the stress during drying, condensation, and template removal. A further advantage of partially disordered films is their isotropy. An advantage of the specific channel-type porosity is the good mechanical integrity [8].

As-synthesized B-type films exhibited very pronounced equidistant peaks in the SAXS analysis. The peaks represent X-ray beams diffracted perpendicular to the film plane (Fig. 3a). This indicates a layered structure with layers ordered parallel to the film surface with a  $d$ -spacing of 8 nm. In the diffraction pattern of calcined B-type films (Fig. 3b), one sharp diffraction spot at  $2\theta = 3.1^\circ$  was still visible. This means that the layer structure remained stable during calcination. The layer spacing decreased to 3 nm, which means shrinkage to 38%.

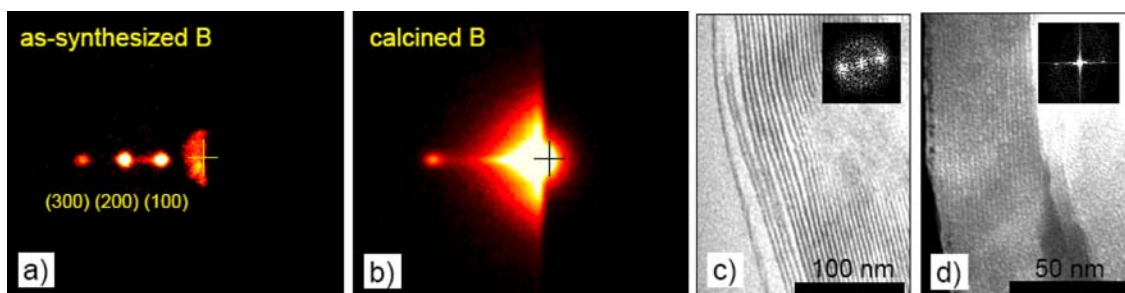


**Fig. 3** (online colour at: [www.pss-a.com](http://www.pss-a.com)) Structure determination of B-type films. a) The SAXS diffraction pattern of as-synthesized and b) calcined films. Sharp diffraction spots out of film plane indicate layers ordered parallel to the substrate, which remain stable upon calcination. The layers are clearly resolved in the TEM micrographs of the cross-sections of c) as-synthesized and d) calcined B-type films. Insets: FFT [8].

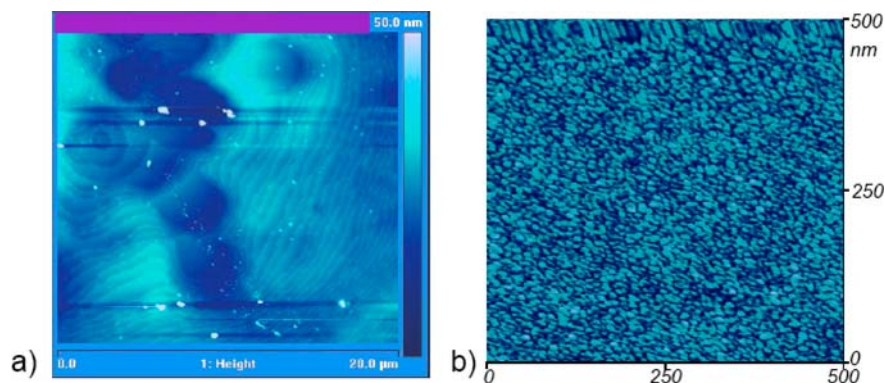


**Fig. 4** (online colour at: [www.pss-a.com](http://www.pss-a.com)) a) AFM height image of a defect of a calcined B-type film. It reveals nano-terraces with a spacing of 3 nm. The image size is  $20 \times 20 \mu\text{m}^2$ . b) AFM phase image of the surface with higher lateral resolution. The phase angle variations are in the  $20^\circ$  range. The distance between the dark regions is approximately 20 nm.

In the TEM images of the B-type films, the layers can be made visible (Fig. 3c and d). Tilting the sample during the investigation did not reveal any additional structure. A calcination-stable layer structure is a surprise, because one expects a collapse of the interlayer spacing after template removal. Such a structure can only be stable if there is a sustaining system among the layers. Although B-type films are not suitable as low- $n$  substrates, their internal layer structure is very interesting in itself.

Examination of the defects in the B-type films with AFM revealed terraces (Fig. 4a). They are visible in about 70% of all investigated defects performing hard tapping mode. These nano-terraces have a step height of 3 nm, which is in a very good agreement with the TEM and SAXS results.

In-between the defects and on each terrace step the surface is very flat ( $\text{RMS} < 0.5 \text{ nm}$ ). However, the AFM phase image reveals some pronounced lateral variations. Figure 4a shows a dark network which can be assigned to higher energy dissipation. This network might be a picture of the sustainers that support the separated layers. In [8] we describe a model resulting in higher dissipation on the top of the sustainers compared with the dissipation on the bridges between them. Therefore we interpret Fig. 2b as a picture of the sustaining network between the simple silica layers.

Based on this interpretation a layered structure with novel kind of sustainers is drafted for the B-type films in Fig. 5b. Flat voids of a typical size of about  $20 \times 20 \times 2 \text{ nm}^3$  occur among the layers. The special structure of the B-type films is likely responsible for some of their peculiarities. The typical macroscopic defects of these films could be ascribed to shrinkage problems during film condensation. On a solid support, a parallel lamella has no possibility to relax when it shrinks, except the formation of a defect. Furthermore, we observed in the TEM micrographs also single lamellas produced by the stress during mi-

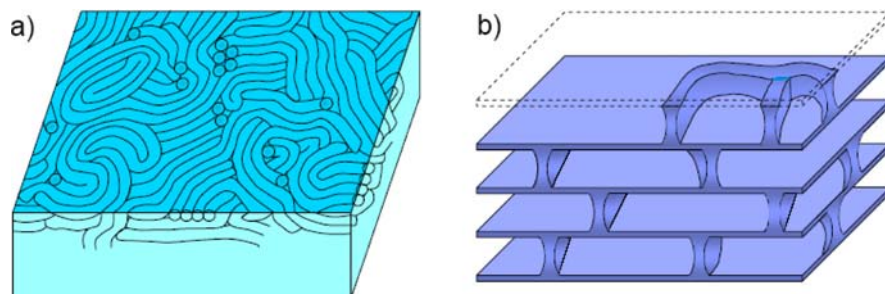


**Fig. 5** (online colour at: [www.pss-a.com](http://www.pss-a.com)) Structure models of mesoporous silica films: a) worm-like structure for the A-type films and b) layer structure with sustainers for B-type films.

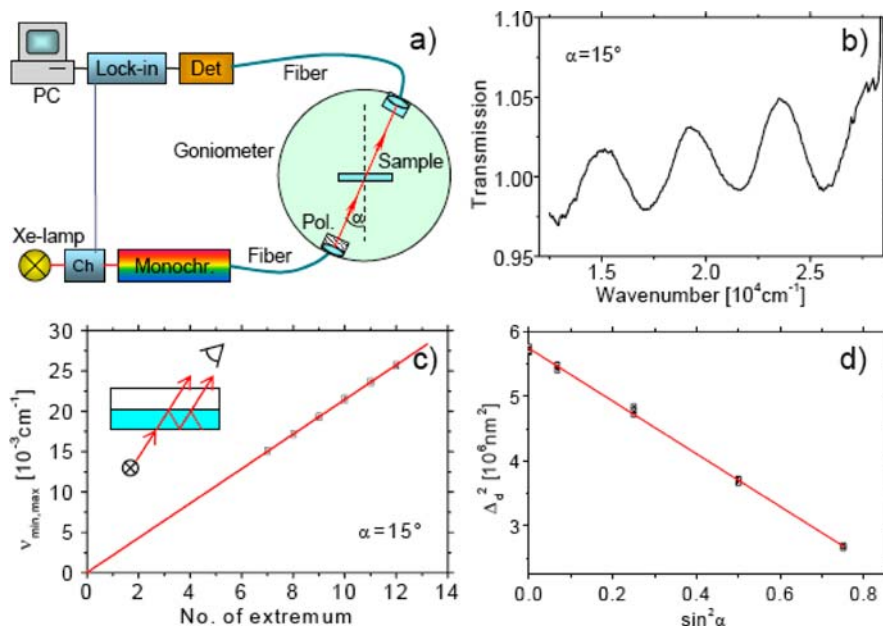


**Fig. 6** (online colour at: [www.pss-a.com](http://www.pss-a.com)) a) Experimental setup of the goniometer for the simultaneous measurement of film thickness and refractive index. The incidence angle  $\alpha$  was varied in the range  $0^\circ$ – $60^\circ$ . b) An example of the measured transmission spectra for the incidence angle  $\alpha$  of  $15^\circ$  with s-polarized light. c) Position of the extremum versus the number of the extremum for  $\alpha = 15^\circ$  for s-polarized light. This graph allows the determination of the thickness dependent part  $\Delta_d$  of the optical path difference. As indicated in the inset, different rays contribute to the transmitted signal. They have an optical path difference  $\Delta$ . d) Determination of the refractive index  $n$  and film thickness  $d$  from the dependence  $\Delta_d$  on  $\alpha$  [13].

crotoning. This fact points to a reduced integrity between the lamellas, which is consistent with the relatively large typical distance between sustainers of 20 nm.

### 2.3 Optical properties of MSFs

The refractive index of calcined A-type films was determined from the interferometric measurements using a two-axes goniometer (Fig. 6a). An example of the measured transmission spectra a special different incidence angle is shown in Fig. 6b. The interference at the thin layer results in different reflection intensities for different wavelengths of light (Fabry–Pérot oscillations). The interference curves have a cos-like shape with intensity variations between 2 and 10%. The positions of the interference extrema on the wavenumber scale have a linear dependence on the interference order. Therefore, this dependence was fitted with a straight line for each incidence angle (Fig. 6c). Also the maximal and minimal possible values for the extrema were considered for the error determination. The slope of this line  $m$  delivers the thickness-dependent part of the optical path difference  $\Delta_d = (2m)^{-1}$ . It differs from the total path difference  $\Delta$  by a reflex pronounced on phase jump:  $\Delta = \Delta_d + \lambda/2$ . Figure 6d shows the dependence of  $\Delta_d$  on the incidence angle for s-polarized light. Mathematically, it is described by [11]:

$$\Delta_d = 2d\sqrt{n^2 - \sin^2 \alpha} . \quad (1)$$

Therefore, the axes have been chosen appropriately to allow a linear fit. This fit enables simultaneous determination of the film thickness  $d$  and the refractive index  $n$ . A refractive index of  $n = 1.18 \pm 0.01$  was determined in the visible range of 350–800 nm. This is one of the lowest measured  $n$  for a transpar-

ent material suited as waveguide support. The air filling fraction, i.e. porosity, of these mesoporous films was calculated using effective medium approximation from Bruggemann [12] to  $(59 \pm 2)\%$ .

Angle-dependent interferometric measurements enable reliable information on the accuracy of the  $n$ -determination and deliver an  $n$ -value averaged over the whole film thickness. The difference in the refractive index for parallel polarized light and perpendicular polarized is unfortunately within the experimental error (0.01), which is, therefore, the upper limit for the birefringence of A-type films.

Stability of the refractive index upon humidity changes and ageing is important for the application of calcined A-type films as low- $n$  substrates. For this a sample was first stored in the desiccator at low humidity of about 30% for 107 days and the refractive index was measured with the previously described method to be  $n = 1.183 \pm 0.003$ . Then, the sample was stored in the desiccator at 57% RH for 17 days, further 6 days at 97% RH and additional 18 days at 97% RH. The resulting refractive indexes were  $n = 1.181 \pm 0.006$ ,  $n = 1.190 \pm 0.017$  and  $n = 1.185 \pm 0.012$ , respectively. It seems that exposition of calcined mesoporous films to higher humidity, as well as the ageing in the period of few months do not influence the refractive index significantly. The measured deviations are within the error bars.

In waveguides, a considerable part of the radiation power is guided in the evanescent field penetrating into low- $n$  support. Therefore, it is very important that the damping due to scattering in the support is low. One possibility to estimate these losses is to measure the diffuse reflectance of these films. Diffuse reflectance spectra were measured using a UV-vis spectrometer with a praying mantis attachment. By this tool the specular reflection was eliminated and only the diffuse reflection was collected. B-type films show a high wavelength-dependent scattering up to  $S = 0.2$  (20%) as expected from the visual impression. Contrary to this result the optical scattering  $S$  of the calcined A-type films was very low,  $S = 0.0026$  (0.26%). However, this value was close to the detection limit of our set-up and may be an overestimation. Having this restriction in mind, we take the value as the basis for the estimation of the scattering coefficient  $\alpha_{sc} = -(1/l) \log_{10}(1-S) = 8.4 \text{ cm}^{-1}$  (in analogy to the absorption coefficient [14]). Furthermore, one can take this value for the estimation of the waveguide damping with such substrates. Assuming that 10% of the modes are guided in the substrate one obtains  $\alpha_{WG} = 0.84 \text{ cm}^{-1}$ . This allows for sure mm-long applications but also guiding over centimeters can be possible which is agreement with our former waveguide experiments [9]. The possible mistake in this estimation (systematic overestimation) would enable a wider application range.

#### 2.4 Synthesis mechanism

The fabrication procedure used in this work is a special version of the SBA-15 synthesis class [7] for mesoporous materials. In several works [15, 16] the synthesis mechanism was discussed with the main focus on the role of the SDA and the surface charge matching possibilities. Although the deeper understanding of the chemical mechanism was not the aim of this work, it gave some new insights in respect to the mechanism.

Experimentally, two surprising facts have been recognized. First, the structure types of the products are more variable than expected. Especially the lamellar structure of the B-type films has not been observed before and cannot be considered as a disturbed variant of a "SBA-15 main structure". Therefore, the abbreviation used for labeling mesopores (here SBA-15) should better be used for the description of the main features of the synthesis and not to assign a structure. A similar non-uniqueness of the structure has been found for the SBA-3 type mesopore synthesis as well [17]. Second, the obtained structure sensitively depends on processing conditions. The same chemical composition of the coating solution leads to different structure types. It seems that the SDA is not able to drive the condensation process efficiently into a unique energetic minimum state.

These two findings are not in a good agreement with the general concept of the SDAs. This concept assumes that the structure-directing agents can control the pore structure of the synthesized material. In our case they form micelles which should determine the film structure. Normally, this concept gives a good guideline for finding new synthesis schemes. However in detail, it cannot be completely right. It can especially not explain strong sensitivities towards processing conditions.

The key for understanding of the synthesis seems to us the fact that the synthesis process goes through a series of non-equilibrium states. The synthesis tries to reach an energetic minimum state determined by the SDA, but because of the simultaneous silica condensation, it is not able to reach this state. Therefore, the synthesis results in a product which is frozen-in somewhere on an assumed reaction path to the ideal structure. The known dependence of the silica condensation on the processing conditions is transferred to the formation of the pore structure. Although our structure-directing agent drives the structure towards one equilibrium state, slightly varying processing conditions lead to the formation of different film types.

The exact description of such processes is difficult. A schematic picture can be given based on the equilibrium phase diagrams. They describe which phase the micelles (separated spherical micelles, hexagonal arrangements of rod-like micelles etc.) form for certain compositions of the solution. However, they neglect that a certain time is needed to reach these phases. Nevertheless, a reaction path in such a diagram can provide a rough explanation for the observed phenomena. The SBA-15-relevant micelle structures formed by the ternary copolymer-water-oil system were described in phase diagrams, e.g. in Ref. [18]. The chemical recipe for the dip-coating solution determines a starting point in this diagram and the chemical composition of the dried film gives an end point. Inbetween these two points there is the reaction path determined by the evaporation of the solvents. However, the structural forecast at the end point is not relevant because of the freezing-in of the structural transformations somewhere on the reaction path. We discussed the possible phenomena of our special system in a former paper [8] and refer to it for the details.

Although the synthesis mechanism is very complex because of the non-equilibrium phenomena, the practical synthesis turned out to be reproducible and controllable. It enables a wider range of products than normal near-equilibrium syntheses, it allows fine-tuning, but it requires careful control of the processing conditions.

### 3 MSFs as substrates for waveguide structures

#### 3.1 Polymer waveguides

Because of the very low refractive index, low optical scattering, sufficient thickness of the films, and the very smooth surface, A-type films are very well suited as ultra-low refractive index substrates, especially for 2D photonic crystal waveguides (PhC WGs). An example of such system is shown in Fig. 7 representing the result of a common project of the TU Hamburg-Harburg, IPHT Jena and MPI Mülheim. A-type films with a thickness of 1  $\mu\text{m}$  were deposited onto oxidized silicon wafers for the fabrication of this waveguide structure. A slab waveguide was produced by spin coating a polymer poly(methyl methacrylat/disperse red-1) (P(MMA-DR1)) with  $n = 1.54$  onto this substrate. Then 2D PhC structures

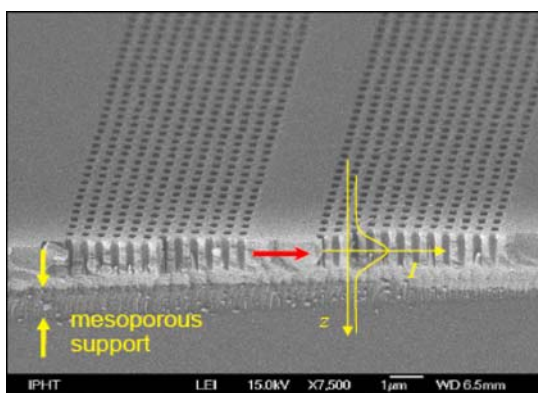


**Fig. 7** (online colour at: [www.pss-a.com](http://www.pss-a.com)) SEM micrograph of the realized 2D PhC LD resonator made of P(MMA/DR-1) on an A-type mesoporous silica film as a support [9]. A schematic drawing shows the field distribution in a guided mode (arrow). The evanescent field of the guided mode penetrates into the support up to some 100 nm.

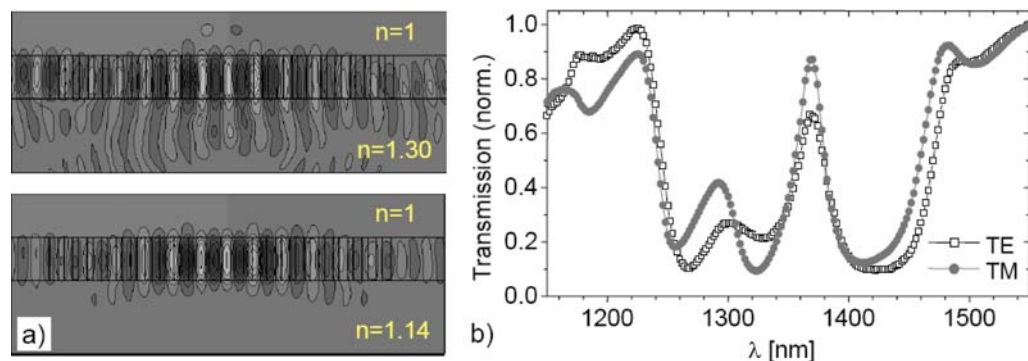


**Fig. 8** (online colour at: [www.pss-a.com](http://www.pss-a.com)) Wave propagation in polymer waveguides [9]. a) Simulations of the electric field distribution inside a finite 2D PhC line defect resonator for two different substrates: Teflon with  $n = 1.3$  and MSF with  $n = 1.14$ . b) Experimental transmission spectra of a P(MMA/DR-1)/MSF line defect resonator for TE-like and TM-like modes.

were fabricated by a combination of different etching processes (EBL, RIE, dry etching) [19, 9]. They formed a resonator consisting of a line defect (LD) in a 2D PhC. In the shown example only the core layer was etched and the air holes do not penetrate the substrate. The resonator consists of two finite square arrays of holes separated by a non-structured region. A 150 nm hole radius was chosen resulting in an optical stop band around the vacuum wavelength of 1.3  $\mu\text{m}$ . The lattice defect is formed by omitting 4 lines of holes perpendicular to the wave propagation direction. The exact design of the structure was optimized by simulations using a 3D finite integration technique as described in [9]. Two examples of the calculated electrical field distributions for finite 2D PhC are depicted in Fig. 8a. The light is strongly confined inside the PhC waveguide core when the ultra-low index substrate is used.

The transmission spectra (Fig. 8b) of this resonator were measured for different polarizations by the prism coupling method. The resonator structure on the mesoporous substrate showed a high transmission in the resonance peak of about 60% for TE and 80% for the TM polarization. These values were expected from the simulations and exceed values determined on similar structures on conventional Teflon supports. A further interesting property of this transmission spectrum are the seemingly absent radiation losses at the air band side of the band gap. The transmission has the same height at this band edge as at the dielectric edge. In contrast, the PhC waveguides on Teflon showed strong losses at the air band edge since these states are above the light cone [9].

Beside the simulations, also simpler considerations can be used to understand the measured result. The decay of the guided modes into the support is schematically depicted in the Fig. 7. The depth of decay depends on the mode type, waveguide thickness, and significantly on the refractive index of the support. This effect can be estimated by a lower limit of the field decay. The fields of every guided mode of a waveguide decay slower into the support than  $\exp\{-z 4\pi(n_0^2 - n_{\text{sup}}^2)^{1/2}/\lambda_0\}$ . Here,  $z$  is the distance from the waveguide-support interface,  $n_0$  the effective refractive index of the waveguide,  $n_{\text{sup}}$  the refractive index of the support, and  $\lambda_0$  the wavelength of the used light [20]. This estimation delivers the result that a 1  $\mu\text{m}$  thick mesoporous film can be sufficient for the field confinement, but not a Teflon film with  $n = 1.3$ , since there is still a remarkable field intensity at 1  $\mu\text{m}$  which can be absorbed or irradiated.

### 3.2 $\text{Ta}_2\text{O}_5$ waveguides and 2D PhC structures

Waveguides made of inorganic materials especially of oxides are regarded to have a wider application range than polymeric ones. They are transparent in larger parts of the spectrum, can resist higher temperatures, and – most importantly – can have larger refractive indices. However, their structuring in the nm-range seems to be generally more difficult. In respect to our low- $n$  supports, it is not clear if such layers are compatible with the support. The inorganic layers will likely create a large stress on the sup-

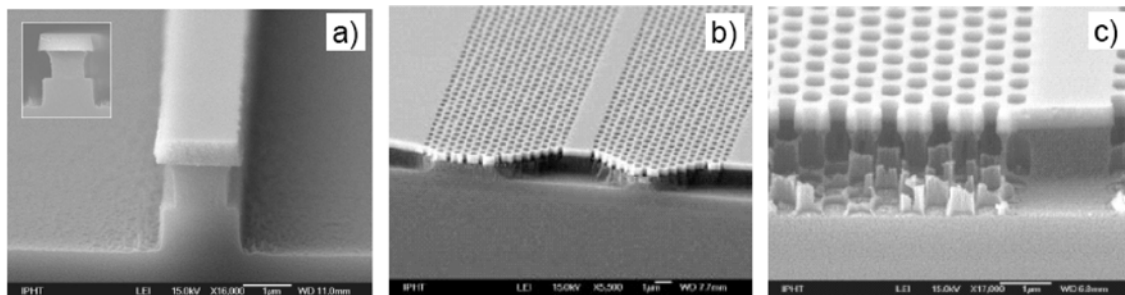


**Fig. 9** Examples for WG structures on MSF supports. a) Strip waveguide, b) PhC WG on a homogeneous support, c) PhC WG on a structured support.

port during their deposition as well as during their structuring. Therefore, we studied some model examples and show the results obtained with  $\text{Ta}_2\text{O}_5$  top-layers here.

Films of  $\text{Ta}_2\text{O}_5$  have been sputtered on the MSFs (mso Jena Mikroschichtoptik GmbH). The structuring of these films was performed in a similar manner as for polymers, but with changed processing parameters. It required tempering at 180 °C after the photoresist deposition and heating during structuring (RIE) to 180 °C together with HF heating from the top. Surface temperatures of 200 °C were likely reached in this step.

The deposition of the original  $\text{Ta}_2\text{O}_5$  layers worked without visible problems. Here, it might have been useful that a surface barrier [21] can protect the porous films against penetration of  $\text{Ta}_2\text{O}_5$  precursors and that the elasticity of the MSF can help to distribute the stress in the forming  $\text{Ta}_2\text{O}_5$  layer. Difficulties occurred in some of the structuring steps resulting in delamination of the layer system. We ascribe these difficulties to water which was adsorbed during sample handling. It was possible to avoid these effects and to demonstrate the fabrication of several structures suitable for stripe waveguides, PhC waveguides, PhC WG bends, and for PhC WG splitters.

A planar stripe waveguide is shown in Fig. 9a. Here, the mesoporous support shows an interesting under-etching effect. Such an effect is not negative for the desired function as waveguide and is likely caused by the very low density of the MSF. Figure 9b shows a PhC waveguide. Here, the etching was stopped at the MSF/ $\text{Ta}_2\text{O}_5$  interface. Alternatively, the etching can be continued deeply into the support as shown in Fig. 9c. The under-etching effect leads then to very thin ribs under the  $\text{Ta}_2\text{O}_5$ . Interestingly, the whole layer arrangement kept stable. It is, up to now, unclear if the remaining rib consists of unchanged mesoporous material or if it is subjected to a densification process during the ion treatment. Such modifications have been observed in the interaction with other ions [22].

The optical characterization of the fabricated structures is still in progress. However, they all fulfilled their principle function in a similar manner as reference structures on glass. There was not observed any additional damping for the fabricated structures originating from the scattering in the mesoporous support. The detailed parameters (bend damping, waveguide damping, and coupling efficiencies) differ of course from the reference structures since the MSF has another refractive index.

These results with the  $\text{Ta}_2\text{O}_5$  system show that a highly accurate structuring of inorganic top-layers on MSFs is possible. This means that the MSFs can resist the larger processing stress in comparison to the requirements for polymer waveguides. This enables future prospects to use the MSF also in high contrast PhC systems. Especially the optical up-down symmetry can be useful in such systems.

### 3.3 PZT films

The incorporation of active materials into waveguides and PhCs is a field of strong interest. The materials should be switchable, nonlinear-optical, or amplifying. They can be incorporated as guests or as constituent of the PhC itself. For example, an electro-optic PhC would be very interesting. However, no material with high electro-optic coefficients and sufficient possibilities for structuring in PhCs has been

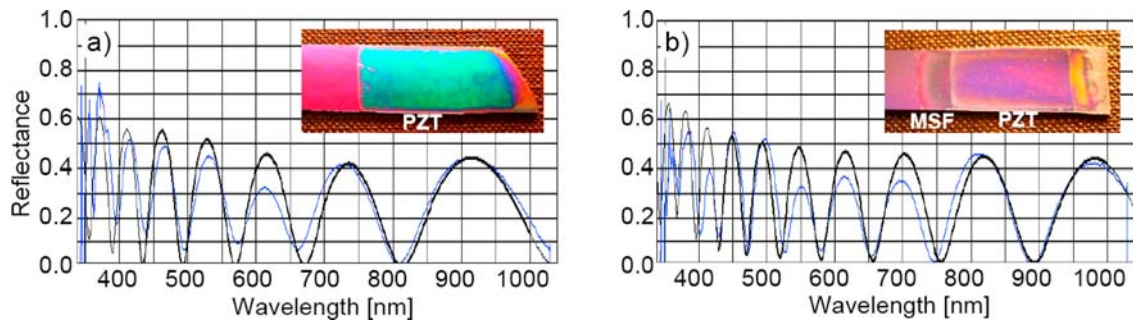


**Fig. 10** (online colour at: [www.pss-a.com](http://www.pss-a.com)) Measured and calculated reflection spectra of a PZT film on Si-wafer (a) and of PZT on a mesoporous silica film (b). Insets are photographs of PZT on Si-wafer and on MSF, respectively. The photographs of the calcined samples were made using a digital camera with diffuse sample illumination.

identified up to now. Films of lead-zirconate-titanate (PZT) could be one promising candidate for that. Ferroelectric inorganic films, especially  $\text{Pb}(\text{Zr}_x\text{Ti}_{1-x})\text{O}_3$  (PZT) are known to have large optical nonlinearities and can be prepared by different methods. The sol-gel approach can be very useful, because it is offering a number of tuning possibilities. In addition, this approach seems to be compatible with the MSF support fabrication. Therefore, this approach was used and investigated concerning the fabrication of PZT/MSF layer structures.

The coating solution for the lead zirconate titanate (PZT) films was prepared as described in Ref. [23]. The PZT precursor solution was deposited onto diverse substrates in the same manner as mesoporous silica films. The temperature in the chamber was 21–23 °C and the humidity varied in the range of 37–50% RH without noticeable influence on the optical appearance of the films in normal and microscopical observation.

The calcined films were transparent and clear (Fig. 10). However, closer observation with optical and electron microscopes reveals a more or less dense crack network on normal supports (Fig. 11a). The cracks develop as a reaction to the stress in the film on firing as it has been discussed in many publications, e.g. [24]. To avoid this polyvinylpyrrolidone (PVP) was added to the coating solution as a stress-relaxing agent. Although the crack formation was reduced by addition of PVP, it could not be fully eliminated. We assign this fact to the different thermal expansion coefficients of PZT and the support. Therefore, the final tuning of the PZT film properties has to be adjusted to the support system.

PZT films were deposited on the mesoporous silica films in the same manner. They were also transparent and mostly clear. The interference colors, typical for thin films, are visible as shown in the insets

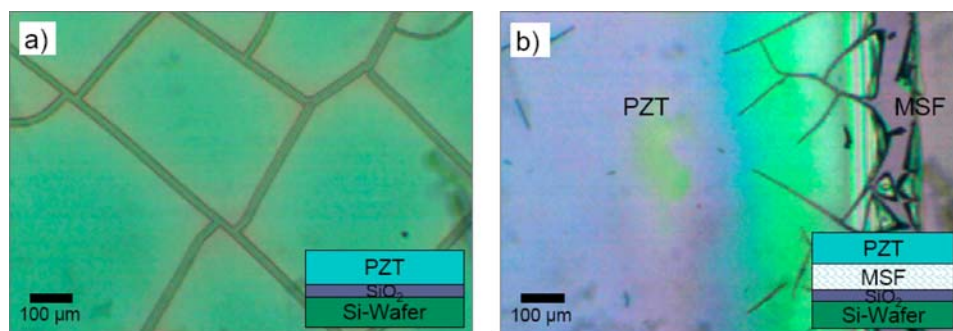


**Fig. 11** (online colour at: [www.pss-a.com](http://www.pss-a.com)) Microscope pictures of a PZT film deposited on a) silicon wafer and b) mesoporous silica film. The photos were made using an eye-piece camera (MA88, CA Scientific Co) with 640 × 480 pixels.

in Fig. 10. The unique color indicates good homogeneity of the films. Only the borders, especially the outflow edge, show different colors, due to changes in the film thickness.

Observation with an optical microscope showed that the PZT films deposited on the MSF have much less cracks, mostly only near to the edges (Fig. 11b). However, the films exhibit slightly blur regions, not visible in the photography and microscope pictures. It is possible that the mesoporous film changed or even crashed during the PZT fabrication. Thickness measurements (Fig. 10) indicated that the thickness  $d$  of the MSF is significantly lower after the deposition of PZT. Such a compression of the film might be caused by infiltration of the PZT precursor. Possibilities to avoid such effects could be the change of surface properties of the MSF or the introduction of surface barriers [21].

The suppression of the regular cracks by deposition on MSF supports is, however, an encouraging result on the way to high-quality PZT films. The flexibility of the porous structure lowers obviously the stress induced in the PZT by the temperature treatment.

## 4 Conclusions

Optically perfect mesoporous films have been synthesized reproducibly. They exhibit an extremely low refractive index, sufficient mechanical and chemical stability, low optical scattering and a thickness up to about 1  $\mu\text{m}$ .

The humidity during film fabrication turned out to be a decisive processing parameter for the fabrication of optically perfect films. In the range between 20 and 40% relative humidity the desired A-type films have been synthesized. The control of the film thickness which is important for many applications is possible via the drawing speed.

Partially ordered mesostructures of worm-like type turned out to have most useful properties (A-type films). They are well suited as low- $n$  supports for waveguides. Low- $n$  supports have three important advantages: one can avoid working with leaky modes, the penetration depth into the substrate is lower, and the system is nearly symmetric (or fully symmetric with a low- $n$  cover layer). This leads to a decoupling of TE and TM modes, which is also very useful for an easier design of functional waveguide structures.

The mesoporous films resist many fabrication procedures for waveguide overlayers. In some cases they may be even advantageous for obtaining high-quality homogeneous overlayers.

**Acknowledgements** The authors thank H.L. Li, H. Bretinger, and R. Brinkmann for experimental support and M. Eich for stimulation of these works. Funding by the DPG is gratefully acknowledged.

## References

- [1] R. D. Miller, *Science* **286**, 421 (1999).
- [2] A. Jain, S. Rogojevic, S. Ponoht, N. Agarwal, I. Matthew, W. N. Gill, P. Persans, M. Tomozawa, J. L. Plawsky, and E. Simonyi, *Thin Solid Films* **398/399**, 513 (2001).
- [3] S. Baskaran, J. Liu, K. Domansky, N. Kohler, X. Li, C. Coyle, G. E. Fryxell, S. Thevuthasan, and R. E. Williford, *Adv. Mater.* **12**, 291 (2000).
- [4] C. T. Kresge, M. E. Leonowicz, W. J. Roth, J. C. Vartuli, and J. S. Beck, *Nature* **359**, 710 (1992).
- [5] J. S. Beck et al., *J. Am. Chem. Soc.* **114**, 10834 (1992).
- [6] C. J. Brinker, Y. Lu, A. Sellinger, and H. Fan, *Adv. Mater.* **11**, 579 (1999).
- [7] D. Zhao, J. Feng, Q. Huo, N. Melosh, G. H. Frederickson, B. F. Chmelka, and G. D. Stucky, *Science* **279**, 548 (1998).
- [8] D. Konjhdzic, H. Bretinger, U. Wilczok, A. Dreier, A. Ladenburger, M. Schmidt, M. Eich, and F. Marlow, *Appl. Phys. A* **81**, 425 (2005).
- [9] M. Schmidt, G. Boettger, M. Eich, W. Morgenroth, U. Huebner, H. G. Meyer, D. Konjhdzic, H. Bretinger, and F. Marlow, *Appl. Phys. Lett.* **85**, 16 (2004).
- [10] See e.g.: D. Grosso, F. Carnol, G. Soler-Illia, E. L. Crepaldi, H. Amenitsch, A. Brunet-Bruneau, A. Bourgeois, and C. Sanchez, *Adv. Funct. Mater.* **14**, 309 (2004).
- [11] L. Bergmann and C. Schäfer, *Lehrbuch der Experimentalphysik Band III* (Walter de Gruyter, Berlin–New York, 1987), p. 344.

- [12] D. A. G. Bruggeman, *Ann. Phys. (Leipzig)* **24**, 636 (1935).
- [13] D. Konjhodzic, H. Bretinger, and F. Marlow, *Thin Solid Films* **495**, 333 (2006).
- [14] See e.g.: D. Wöhrle, M. W. Tausch, and W.-D. Stohrer, *Photochemie* (Wiley-VCH, Weinheim, 1998), p. 498.
- [15] D. Zhao, P. Yang, N. Melosh, J. Feng, B. F. Chmelka, and G. D. Stucky, *Adv. Mater.* **10**, 1380 (1998).
- [16] P. C. A. Alberius, K. L. Frindell, R. C Hayward, E. J. Kramer, G. D. Stucky, and B. F. Chmelka, *Chem. Mater.* **14**, 3284 (2002).
- [17] F. Marlow, A. S. G. Khalil, and M. Stempniewicz, *J. Mater. Chem.* **17**, 2168 (2007).
- [18] P. Holmquist, P. Alexandridis, and B. Lindman, *J. Phys. Chem. B* **102**, 1149 (1998).
- [19] U. Huebner, R. Boucher, W. Morgenroth, M. Schmidt, and M. Eich, *Microelectron. Eng.* **83**, 1138 (2006).
- [20] See e.g.: K. Iizuka, *Elements of Photonics*, Vol. II (Wiley-Interscience, 2002).
- [21] M. Stempniewicz, M. Rohwerder, and F. Marlow, *Chem. Phys. Chem.* **8**, 188 (2007).
- [22] M. Stempniewicz, A. Khalil, M. Rohwerder, and F. Marlow, *J. Am. Chem. Soc.* **129**, 10561 (2007).
- [23] S. Takenaka and H. Kozuka, *Appl. Phys. Lett.* **79**, 3485 (2001).
- [24] H. Kozuka, S. Takenaka, H. Tokita, and M. Okubayashi, *J. Eur. Ceram. Soc.* **24**, 1585 (2004).